JGR Solid Earth

RESEARCH ARTICLE
10.1029/2020JB020835

Gas-Driven Tensile Fracturing in Shallow Marine Sediments

Hugh Daigle[1,2], Ann Cook[3], Yi Fang[4], Abhishek Bihani[1,2], Wen Song[1,2], and Peter B. Flemings[4,5]

[1]Center for Subsurface Energy and the Environment, The University of Texas at Austin, Austin, TX, USA, [2]Hildebrand Department of Petroleum and Geosystems Engineering, The University of Texas at Austin, Austin, TX, USA, [3]School of Earth Sciences, The Ohio State University, Columbus, OH, USA, [4]Institute for Geophysics, Jackson School of Geosciences, The University of Texas at Austin, Austin, TX, USA, [5]Department of Geological Sciences, Jackson School of Geosciences, The University of Texas at Austin, Austin, TX, USA

Key Points:

- Gas-driven tensile fracturing can occur in the upper 40 m below seafloor if the clay-sized fraction is greater than 20%
- If the clay-sized fraction exceeds 60%–70%, gas saturations <10% can generate tensile fractures in sediments as deep as 2 km below seafloor
- Hydrate dissociation can cause fracturing and venting where the base of the hydrate stability zone intersects the seafloor

Correspondence to:
H. Daigle,
daigle@austin.utexas.edu

Citation:
Daigle, H., Cook, A., Fang, Y., Bihani, A., Song, W., & Flemings, P. B. (2020). Gas-driven tensile fracturing in shallow marine sediments. *Journal of Geophysical Research: Solid Earth*, *125*, e2020JB020835. https://doi.org/10.1029/2020JB020835

Received 21 AUG 2020
Accepted 20 NOV 2020

Abstract The flow of gas through shallow marine sediments is an important component of the global carbon cycle and affects methane release to the ocean and atmosphere as well as submarine slope stability. Seafloor methane venting is often linked to dissociating hydrates or gas migration from a deep source, and subsurface evidence of gas-driven tensile fracturing is abundant. However, the physical links among hydrate dissociation, gas flow, and fracturing have not been rigorously investigated. We used mercury intrusion data to model the capillary drainage curves of shallow marine muds as a function of clay content and porosity. We combined these with estimates of in situ tensile strength to determine the critical gas saturation at which the pressure of the gas phase would exceed the pressure required to generate tensile fractures. Our work showed that fracturing is favored in the shallowest 38 m of sediment when the clay-sized fraction is 0.2, but fracturing may be possible to a depth of 132 m below seafloor (mbsf) with a clay-sized fraction of 0.5 and to a depth of nearly 500 mbsf with a clay-sized fraction of 0.7. Dissociating hydrate may supply sufficient quantities of gas to cause fracturing, but this is only likely near the updip limit of the hydrate stability zone. Gas-driven tensile fracturing is probably a common occurrence in the upper 10–20 mbsf regardless of clay-sized fraction, does not require much gas (far less than 10% gas saturation), and is not necessarily an indication of hydrate dissociation.

Plain Language Summary Gas bubble emissions from discrete locations on the seafloor are observed at many locations worldwide. Bubble emissions are often linked to hazards such as submarine landslides and may contribute to ocean acidification and release of methane to the atmosphere. Observations indicate that the gas tends to move through fractures or cracks, but the role of gas in potentially forming those fractures and the overall process of gas accumulation and flow in shallow marine sediments are not well understood. Using a new model based on laboratory data to predict how much gas is needed to generate fractures in shallow marine sediments, we show that gas can easily generate fractures near the seafloor, particularly when the sediments contain a significant amount of clay. Our results demonstrate that gas-driven fracturing is probably a common occurrence near the seafloor, does not require very much gas, and may not necessarily be an indication of gas hydrate melting caused by ocean temperature increase.

1. Introduction

Methane hydrates are ice-like, nonstoichiometric compounds of water and methane that are stable at high pressure and low temperatures, and occur in the shallow subsurface of continental margins and in sediments below permafrost (Ruppel, 2011). There are three research foci associated with methane hydrates: (1) as an energy resource, (2) as a large reservoir of carbon with associated roles in climate change and carbon cycling, and (3) as a potential marine geohazard (Boswell & Collett, 2011; Collett et al., 2015; Maslin et al., 2010; Ruppel & Kessler, 2017). The geomechanical aspects of methane hydrate formation and associated gas migration in marine sediments have been an active area of research for many years (e.g., Daigle & Dugan, 2010b; Fauria & Rempel, 2011; Flemings et al., 2003; Hornbach et al., 2004; Jain & Juanes, 2009; Nimblett & Ruppel, 2003; Stranne et al., 2017; Xu & Germanovich, 2006). Particular interest has been given to hydrate that occurs as a filling in fractures and veins (Cook & Goldberg, 2008; Cook et al., 2008,

2014; Daigle & Dugan, 2010b, 2011; Jin et al., 2015; Nimblett & Ruppel, 2003). These features tend to occur predominantly in clay-rich sediments, suggesting that they are related to low permeability and associated elevated fluid pressures (Daigle & Dugan, 2010b, 2011; Ginsburg & Soloviev, 1997; Sassen et al., 2001; Weinberger & Brown, 2006), or that they form as a result of capillary forces inhibiting nucleation of disseminated hydrate within the pore space (Clennell et al., 1999; Cook et al., 2014; Rempel, 2011; You et al., 2019). The prospect that marine sediments may fail in tension or shear due to pore pressures associated with fluid flow and methane hydrate dissociation has significant implications for hydrates as a geohazard and release of methane to the water column.

Gas-driven tensile fracturing in association with methane hydrates has been investigated or suggested by many authors (Choi et al., 2011; Daigle & Dugan, 2010a; Daigle et al., 2011; Flemings et al., 2003; Holtzman & Juanes, 2011; Hustoft et al., 2009; Jain & Juanes, 2009; Liu & Flemings, 2007; Natzeband et al., 2005; Rees et al., 2011; Stranne et al., 2017; Sultan et al., 2014; Sun et al., 2012; Wood et al., 2002; Zühlsdorff & Spiess, 2004). Fractures are high-permeability conduits that can lead to venting of methane at the seafloor (e.g., Hustoft et al., 2009), and can originate within a few meters of the seafloor (Thatcher et al., 2013) or extend tens of hundreds of meters below the seafloor, spanning the entire thickness of the hydrate stability zone (Daigle et al., 2011; Torres et al., 2002). The ability of gas generated from hydrate dissociation to fracture overlying sediments has important implications for predicting feedbacks between ocean warming and methane release (e.g., Archer et al., 2009). Issues relating to gas-driven tensile fracturing extend to marine sediments outside the hydrate stability zone as well, with the movement of gas posing hazards to offshore infrastructure and contributing to sediment-ocean methane exchange (Best et al., 2006). The importance of gas-driven fracturing to shallow gas movement is overall poorly understood due to a lack of predictive models (James et al., 2016).

We used mercury intrusion capillary pressure (MICP) measurements performed on marine sediments from around the world to constrain relationships between capillary pressure and gas saturation, and combined this with estimates of tensile strength to predict the conditions under which gas-driven tensile failure may occur. We show that any amount of gas in the pore space will cause fracturing in sediments as deep as 500 m below sea floor (mbsf) if the fraction of clay-sized grains is larger than 70%, while fracturing will only occur in sediment shallower than 40 mbsf when the clay-sized fraction exceeds 20%. The predictive model we present for variation in capillary pressure curves with porosity and clay-sized fraction allows for detailed predictions of sealing capacity and mode of gas migration in heterogeneous lithologies. We finally demonstrate that hydrate dissociation where the base of the hydrate stability zone intersects the seafloor can easily lead to gas-driven tensile fracturing and bubble emission.

2. Tensile Fracturing and Capillary Drainage

We assume that shallow marine sediments are linearly elastic media with nonzero tensile strength in which tensile fractures can form. This is based on experimental evidence of Johnson et al. (2002, 2012) and Boudreau et al. (2005), among others. For sediments that have undergone some diagenesis, cementation is the most likely source of tensile strength. However, some tensile strength is implied by the results of Johnson et al. (2012) even for marine muds within 20 cm of the sediment-water interface. The tensile strength of these very shallow sediments can probably be attributed to grain arrangement (Johnson et al., 2012) and a combination of electrostatic attraction between the edges and faces of clay minerals and van der Waals attraction (McCave & Hall, 2006; McCave et al., 1995; Russel, 1980). We do not explicitly consider the effect of capillary forces in tensile fracturing by a nonwetting phase (e.g., Shin & Santamarina, 2010), though these could be an important component of tensile strength as well.

In a porous medium saturated with one or more fluids, tensile failure will occur when the fluid pressure exceeds the sum of the minimum principal stress (σ_3) and the tensile strength of the medium (T) (Boudreau, 2012; Jain & Juanes, 2009) (all nomenclature is defined in Table 1). In a water-wet porous medium, a gas phase will always exist at a greater pressure than the water phase, with the pressure difference equal to the capillary pressure. In this situation, the gas phase will tend to be the phase initiating fracturing. The fracturing criterion can thus be written as

Table 1
Nomenclature

Symbol	Definition	Dimensions
a	Initial flaw length	L
c_u	Unconfined compressive strength	M/LT^2
f_c	Mass fraction of solid matrix composed of clay-sized grains	M/M
K_{1C}	Critical mode 1 stress intensity factor	$M/L^{1/2}T^2$
m_i	Hoek-Brown constant	-
P_c	Capillary pressure	M/LT^2
P_e	Capillary entry pressure	M/LT^2
P_g	Gas phase pressure	M/LT^2
P_w	Water phase pressure	M/LT^2
R	Pore radius	L
S_g	Gas saturation	L^3/L^3
S_h	Hydrate saturation	L^3/L^3
S_w	Water saturation	L^3/L^3
S_{wi}	Irreducible wetting phase saturation	L^3/L^3
T	Tensile strength	M/LT^2
$V_{m,g}$	Gas molar volume	L^3/mol
$V_{m,h}$	Hydrate molar volume	L^3/mol
V_p	Compressional wave velocity	L/T
z	Depth below seafloor	L
γ	Gas-water interfacial tension	M/T^2
$\gamma_{CH4,W}$	Methane-water interfacial tension	M/T^2
$\gamma_{Hg,V}$	Mercury-vacuum interfacial tension	M/T^2
$\theta_{CH4,W}$	Contact angle of methane-water interface on solid grains	-
$\theta_{Hg,V}$	Contact angle of mercury-vacuum interface on solid grains	-
λ	Pore-size parameter	-
v	Poisson's ratio	-
σ_3	Minimum principal stress	M/LT^2
σ_h	Total horizontal stress	M/LT^2
σ_h'	Horizontal effective stress	M/LT^2
σ_v	Total vertical stress	M/LT^2
σ_v'	Vertical effective stress	M/LT^2
Φ	Porosity	L^3/L^3

$$P_g > \sigma_3 + T, \tag{1}$$

where P_g is the gas phase pressure. Here, T is assumed to be positive as it represents a strength rather than a stress. Equation 1 may be recast in terms of the capillary pressure P_c by subtracting the water phase pressure P_w from both sides:

$$P_g - P_w = P_c > \sigma_3 - P_w + T. \tag{2}$$

Presumably, the gas phase exists at a capillary pressure greater than or equal to the capillary entry pressure of the pores containing it. However, tensile failure could also occur at capillary pressures below the

capillary entry pressure of the sediment, for example, in the case of failure of a capillary barrier (Ingram & Urai, 1999). Note that the presence of two immiscible fluid phases requires the use of total, rather than effective, stress in Equations 1 and 2, since stress transfer across fluid-fluid interfaces changes the thermodynamic considerations of the relationships between fluid phase pressures and the deformation of the porous medium (Bishop, 1959; Boudreau, 2012; Coussy, 2004, 2007; Nuth & Laloui, 2008). Indeed, if a thin film of water separates gas from the grain surface as expected in a water-wet medium (Hirasaki, 1991), the gas-phase pressure can only act on the rock through the water film, causing a local increase in the water-phase pressure. The use of the total stress removes the need to consider this effect. Equation 2 thus establishes a fracture criterion based on capillary pressure. In a normal faulting stress regime where σ_1 is vertical and σ_3 is horizontal, fractures will open horizontally and propagate vertically. When the stress field is nearly isotropic, that is, $\sigma_1 \approx \sigma_2 \approx \sigma_3$, as may be the case in very shallow sediments (e.g., Boehm & Moore, 2002), there will be no preferential direction of fracture propagation. However, in the special case of gas-driven fracturing, linear elastic fracture mechanics (LEFM) dictate that bubbles in a linear elastic medium like marine sediment will assume the shape of an oblate ellipsoid (Barry et al., 2010) and gas buoyancy will cause the ellipsoid to be oriented with its major axis oriented parallel to the gravitational vector (Algar et al., 2011). Therefore, even in the case of isotropic stresses, gas-driven fractures should tend to propagate vertically.

The capillary pressure of the gas phase is related to the volume fraction of the pore space occupied by gas, which is the gas saturation S_g. As a nonwetting phase, gas must overcome an entry pressure for the curved gas-water interface to enter a pore and displace water. For a cylindrical pore of radius r, the entry pressure P_e for a completely nonwetting fluid is given by Washburn's equation (Washburn, 1921):

$$P_e = \frac{2\gamma}{r}, \tag{3}$$

where γ is the gas-water interfacial tension. Because sediments contain a range of pore sizes, different values of gas pressure will correspond to gas entering pores of different sizes. The capillary drainage curve describes the relationship between gas pressure and gas saturation with the assumption that gas will fill the largest pores at the lowest pressures and move into progressively smaller pores with increasing pressure (Bear, 1972). During primary drainage, wherein the sediment begins fully saturated with water, gas must first overcome the entry pressure of the largest pores. After that, with each pressure increment, it will displace water from any pore that has an entry pressure smaller than or equal to the new capillary pressure and has a connected pathway to existing gas-filled pores (Larson & Morrow, 1981). The value of P_e that satisfies the tensile fracturing criterion in Equation 2 may therefore be related to a critical gas saturation through the capillary drainage curve.

The potential for tensile fracturing due to excess gas pressure can be reduced if the gas pressure can dissipate by porous flow. Flow of a nonwetting phase in a porous medium can only occur if the gas saturation achieves a certain mobility threshold saturation. The mobility threshold depends on many different properties of the sediment, including pore structure and scale of heterogeneities. While numerical and laboratory pore network models have demonstrated that nonwetting phase flow occurs only after the saturation achieves the percolation threshold (Chatzis & Dullien, 1977; Diaz et al., 1987; Ewing & Gupta, 1993; Larson & Morrow, 1981; Lenormand et al., 1983; Sahimi, 2011), experiments on real muds and mudrocks have shown gas breakthrough at saturations far below the percolation threshold (Hildenbrand et al., 2002, 2004; Schowalter, 1979). We define the gas saturation at breakthrough as the mobility threshold. Schowalter (1979) suggested that this saturation is generally 10%, while the experiments of Hildenbrand et al. (2002, 2004) suggest a much lower value around 2%. If the mobility threshold is reached before tensile failure occurs, then pressure can be dissipated by porous flow. The exception to this is the case where the rate of pressure buildup exceeds the rate of dissipation to the point where tensile fracture occurs. We note that our treatment of gas-driven tensile failure considers the coexistence of a wetting and nonwetting phase within a representative elementary volume of a porous medium. We are not considering dynamics of gas ganglia, thin fluid films, or other processes operating at the grain or pore scale. Since the capillary drainage curve is a macroscopic description of the relationship between nonwetting phase pressure and saturation – that is, local variations in capillary pressure due to differences in fluid interface curvature or during Haines jumps are not considered (Bear, 1972; Blunt, 2017) – our approach to the fracturing criterion should be valid. More

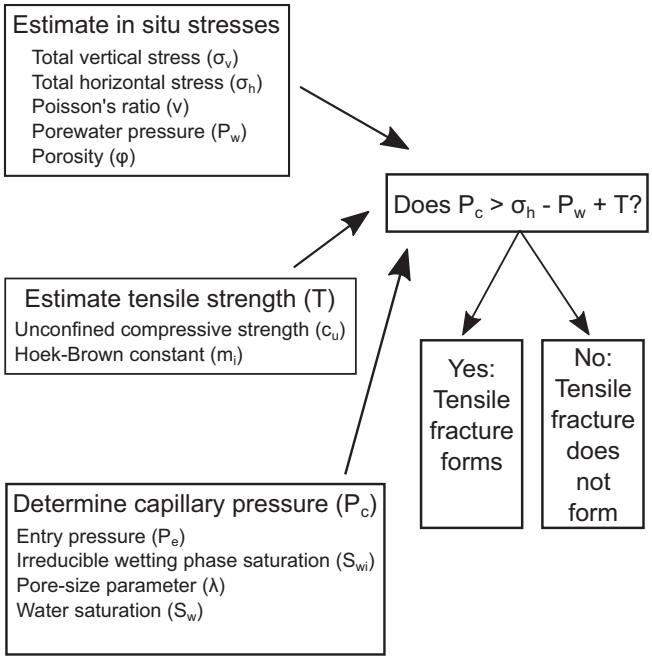

Figure 1. Illustration of process for determining the potential for tensile failure with relevant parameters.

sophisticated models are needed to examine behavior at the grain scale (e.g., Bihani & Daigle, 2019; Jain & Juanes, 2009).

Finally, we note that we do not consider fracture propagation or any dynamic mechanical response after the fracturing criterion is met. Johnson et al. (2002) and Barry et al. (2010), among others, have shown that tensile failure and gas bubble rise in shallow marine sediments is described well by LEFM. There are two pertinent items related to fracturing behavior. First, Algar et al. (2011) and Boudreau (2012) have shown that, after gas initially opens a fracture that then closes, subsequent gas escape will occur preferentially by reactivating the existing fracture surface. The fracture criterion we adopt in this work corresponds to initial fracturing, but it is important to remember that subsequent fracturing will be much easier and occur at lower gas pressures and saturations. Second, the opening of a tensile fracture compresses the surrounding, unfailed sediment, which inhibits additional tensile fracturing in the immediate vicinity of the original fracture due to the local increase in horizontal stress. This phenomenon is known as the stress shadow effect (Warpinski & Branagan, 1989; Warpinski & Teufel, 1987). Tensile fractures will therefore have a characteristic spacing that is related to the material properties of the host sediments. This in turn may limit the gas flow rate as fracture spacing controls fracture system permeability along with fracture aperture (Daigle & Dugan, 2010b).

3. Methods

Determining the potential for gas-driven tensile fracturing requires (1) an estimate of in situ stresses, (2) an estimate of tensile strength, and (3) a capillary drainage curve. An illustration of this process with relevant parameters is shown in Figure 1.

3.1. In Situ Stress Estimation

We considered a generic marine sedimentary setting where the maximum principal stress was vertical (σ_v), and the sediments were vertically transversely isotropic such that the two horizontal stresses were equal to the minimum principal stress σ_h. We emphasize here that these are far-field stresses and not subject to any local perturbations that may arise from the presence of gas. Defining the vertical and horizontal effective stresses as $\sigma_v' = \sigma_v - P_w$ and $\sigma_h' = \sigma_h - P_w$ where P_w is the pore water pressure, from linear elasticity

$$\sigma_h' = \frac{\nu}{1-\nu}\sigma_v', \tag{4}$$

or

$$\sigma_h = \frac{\nu}{1-\nu}\left(\sigma_v - P_w\right) + P_w, \tag{5}$$

where ν is Poisson's ratio. We acknowledge that there is long-standing disagreement in the literature as to how well Equations 4 and 5 represent the true in situ stresses in shallow marine sediments (see the discussion in Zoback [2007]). For example, Eaton (1969) used drilling data from the Gulf of Mexico to back-calculate Poisson's ratio from Equation 4 and found that $\nu < 0.3$ was necessary to fit the data in the shallowest sediments. These values of ν are much lower than typical values for shallow sediments (>0.4 [Hamilton, 1979; Reynolds, 1997]). On the other hand, leak-off test data from shallow sediments in the Gulf of Mexico (Wojtanowicz et al., 2000) and the South China Sea (Yan et al., 2015) indicate that the minimum horizontal stress is very close to the vertical stress ($\sigma_h'/\sigma_v' > 0.8$) which is more consistent with expected values of ν (i.e., $\sigma_h'/\sigma_v' = 0.8$ implies $\nu = 0.44$ from Equation 4). Other work on fracturing in shallow marine

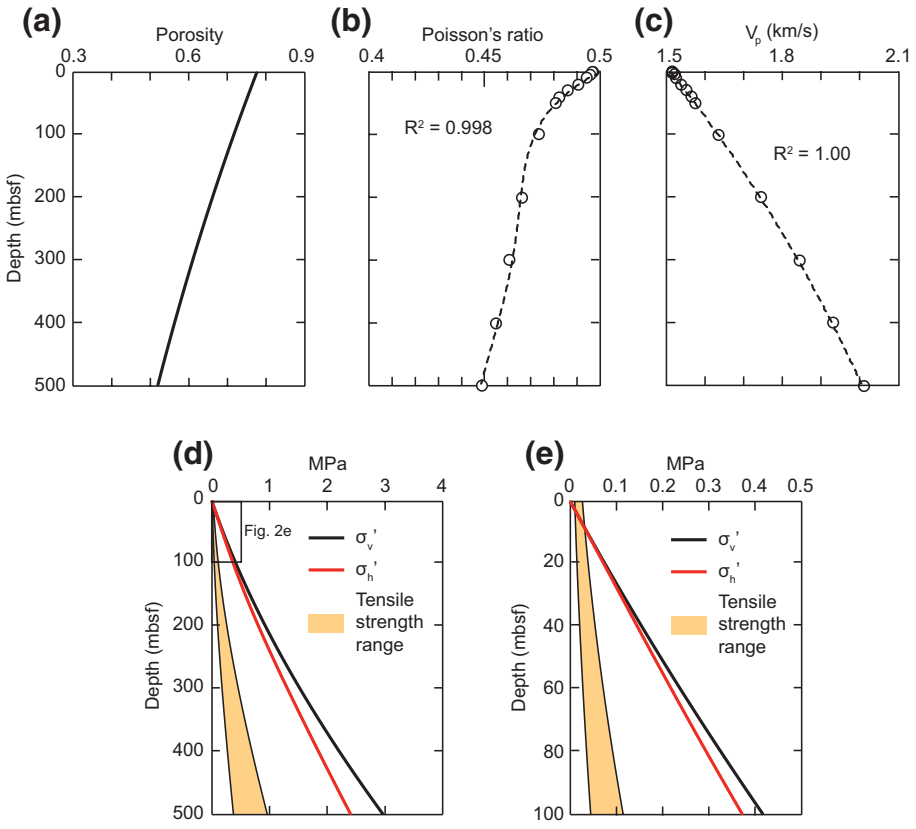

Figure 2. (a) Porosity-depth curve from Kominz et al. (2011). (b) Polynomial fit for Poisson's ratio versus depth. (c) Polynomial fit for compressional wave velocity (V_p) versus depth. Data shown in (b and c) from Hamilton (1979). (d) Vertical and horizontal effective stresses along with range of tensile strength for our generic passive margin sediments. (e) Close-up of (d) showing behavior at shallow depths.

sediments has assumed different σ_h'/σ_v' ratios, for example, constant values of 0.6 (Daigle & Dugan, 2010b) or 0.67 (Daigle & Dugan, 2011). If the true nature of the in situ stresses is unknown, then it simply must be understood that underestimating σ_h, or for that matter neglecting the tensile strength of the sediment, will result in easier fracture generation.

We used the relationship reported by Kominz et al. (2011) for clay to determine porosity φ as a function of depth below seafloor z (m):

$$\varphi = 0.775e^{-\frac{z}{1251}}. \quad (6)$$

Note that this differs from the form of the equation given by Kominz et al. (2011) as it has been modified to yield porosity in decimal rather than percent. Equation 6 is valid for sediments shallower than 500 m below seafloor (mbsf) (Figure 2a). The porosity at 500 mbsf predicted by Equation 6 is 0.52, which is somewhat higher than that predicted by other porosity-depth models for marine clays. For example, the model of Velde (1996) for sediments 0–500 mbsf yields a porosity of 0.38 at 500 mbsf. This is probably an effect of the number of data points used for regression: the model of Velde (1996) is based on data from 7 boreholes whereas the model of Kominz et al. (2011) is based on 53 boreholes, and there is substantial scatter in the latter data set both above and below the line described by Equation 6. Overestimating the porosity would result in an underestimate of both in situ stresses and capillary pressures. After calculating porosity from Equation 6, we determined the bulk density as a function of depth from the porosity with a pore fluid density of 1,024 kg/m^3 and sediment grain density of 2,700 kg/m^3. The vertical effective stress was then calculated by integrating the bulk density with respect to depth with an assumption of hydrostatic pore pressure. To

find σ_h, we determined ν as a function of depth by fitting a sixth-order polynomial to Hamilton's (1979) compilation of ν in shallow marine sediments (Figure 2b), and the total vertical stress was obtained from porosity or bulk density data. We note here that the porosity (Figure 2a), Poisson's ratio (Figure 2b), and compressional velocity (Figure 2c) trends we use are best fits from data with varying clay-sized fractions, so the stresses and tensile strengths we estimate will be average values. In terms of estimating in situ stresses, this probably does not significantly affect the results. Hamilton (1979) also reported Poisson's ratio for shallow, unconsolidated sands, and the values are very close to the values for silty clays that we used. As long as coarser-grained material only makes up a small portion of the sedimentary column so that its lower porosity at shallow depths (Kominz et al., 2011) does not affect the vertical stress, the effect on the estimated horizontal stress will be negligible.

3.2. Tensile Strength Estimation

In the framework of Griffith (1921), marine sediments may be considered as media filled with a number of existing flaws that increase in size and coalesce during fracturing. One method of obtaining the tensile strength in this framework is to determine the mode 1 fracture toughness and make an assumption of initial flaw size, thus determining the tensile strength using LEFM. Many studies have shown that this method can accurately describe the fracture initiation and propagation processes in marine sediments (Algar & Boudreau, 2010; Barry et al., 2010; Boudreau et al., 2005; Johnson et al., 2002, 2012). However, as Boudreau (2012) points out, the initial flaw size in marine sediments is usually unknown, which presents serious challenges in using LEFM as a predictive tool for tensile strength. Therefore, we adopted a simpler method of determining tensile strength based on the Hoek-Brown failure criterion (Hoek & Brown, 1997).

The Hoek-Brown failure criterion is an empirically derived, nonlinear Mohr-Coulomb failure envelope. For intact rocks, the tensile strength T is related to the unconfined compressive strength c_u by

$$T = -\frac{c_u}{2}\left(m_i - \sqrt{m_i^2 + 4}\right), \tag{7}$$

where m_i is the Hoek-Brown constant. Hoek (2006) gives a recommended value of $m_i = 4 \pm 2$ for claystones, and this value is consistent with results of triaxial shear experiments performed on marine muds and mudstones by Silva et al. (2000), Moses et al. (2003), and Dugan and Germaine (2009). Therefore, we used this value for m_i.

To determine c_u, we used the correlation of Ingram and Urai (1999) for muds and mudrocks:

$$\log_{10} c_u = -6.36 + 2.45 \log_{10}\left(0.86 V_p - 1172\right), \tag{8}$$

where c_u is given in MPa and V_p is the compressional wave velocity in m/s. The vertical and horizontal effective stresses, as well as the range of tensile strength predicted from Equation 7, are shown in Figures 2d and 2e. Tensile strength ranges from 18.1 ± 7.92 kPa at the sea floor to 679 ± 297 kPa at 500 mbsf (with uncertainties corresponding to the possible range of m_i). The average value at 500 mbsf is 28% of the horizontal effective stress, and this ratio is relatively constant at 21%–28% from 30 to 500 mbsf, above which the tensile strength corresponds to a greater fraction of the horizontal effective stress.

To assess whether our predicted tensile strengths are reasonable, we compared our results to an estimate derived from the in situ fracture toughness values reported by Johnson et al. (2012) for marine clays. From LEFM, the mode 1 fracture toughness at failure K_{1C} is related to the tensile strength T by

$$T = \frac{K_{1C}}{2}\sqrt{\frac{\pi}{a}}, \tag{9}$$

where a is the half-length of a preexisting disc-shaped flaw (Boudreau, 2012). In our generic marine sediment case, the porosity at seafloor is 0.78 and we predict a tensile strength of 26 kPa. Johnson et al. (2012) show $K_{1C} \approx 100$ Pa·m$^{1/2}$ for clayey silt with similar porosity. From Equation 9, this implies $a = 80$ μm, which

seems reasonable for intact sediments where the largest flaw size is some multiple of the largest grain size. For sediment with porosity of 0.6, we predict $T = 500$ kPa, and using Equation 9 with $K_{1C} = 1{,}000$ Pa·m$^{1/2}$ from Johnson et al. (2012) yields $a = 3$ μm. Our predicted tensile strengths are thus consistent with initial flaw sizes being on the order of grain and pore sizes. We do note that, in the LEFM framework, the tensile strength could be lower if some process like bioturbation created larger flaws. Our estimates probably represent upper bounds on tensile strength.

3.3. Capillary Drainage Curves

We used the Brooks-Corey parameterization of the capillary drainage curve:

$$P_c\left(S_w\right) = P_e\left(\frac{S_w - S_{wi}}{1 - S_{wi}}\right)^{-\frac{1}{\lambda}}, \tag{10}$$

where S_w is the wetting phase saturation (assumed to be water), S_{wi} is the irreducible wetting phase saturation, P_e is the capillary entry pressure, and λ is the pore-size parameter (Brooks & Corey, 1964). To constrain the Brooks-Corey parameters (P_e, S_{wi}, and λ), we used previously published MICP measurements performed on natural and resedimented samples of marine muds from various locations around the world (Daigle & Dugan, 2014; Daigle et al., 2019; Reece et al., 2013; Sawyer et al., 2008; Schneider, 2011). The Brooks-Corey parameters are expected to vary with grain size and porosity. We found the following correlations for P_e and λ:

$$\ln P_e = \left(6.59 \pm 0.584\right)\left(1 - \varphi + S_{wi}\right)f_c - \left(2.76 \pm 0.224\right), \tag{11}$$

where P_e is in MPa, φ is the total porosity (determined independently for all samples by the moisture-and-density method), and f_c is the mass fraction of the solid matrix composed of clay-sized grains (smaller than 2 μm in diameter). Equation 11 calculates P_e for methane invading a water-saturated pore, while the pressures measured in the MICP tests correspond to mercury entering an evacuated pore. The mercury pressures were converted to equivalent methane-water pressures by multiplying by $-(\gamma_{CH4,W}\cos\theta_{CH4,W})/(\gamma_{Hg,V}\cos\theta_{Hg,V})$ where $\gamma_{CH4,W}$ is the methane-water interfacial tension (0.072 N/m), $\theta_{CH4,W}$ is the contact angle of the methane-water interface on solid grains (0°) (Henry et al., 1999), $\gamma_{Hg,V}$ is the mercury-vacuum interfacial tension (0.480 N/m), and $\theta_{Hg,V}$ is the contact angle of the mercury-vacuum interface on solid grains (140°) (Purcell, 1949). The minus sign in this expression is necessary since $\cos\theta_{Hg,V} < 0$. The correlation for the pore-size parameter was found to be

$$\ln \lambda = \left(1.64 \pm 0.162\right)f_c - \left(0.921 \pm 0.0774\right). \tag{12}$$

These correlations had R^2 of 0.81 (Figure 3a) and 0.46 (Figure 3b), respectively. The reported errors in the regression coefficients are ±1 standard deviation.

The S_{wi} determined from an MICP test is not the true irreducible wetting phase saturation (i.e., the wetting phase volume fraction trapped irretrievably by capillary forces) because during the MICP test mercury (assumed to be the nonwetting phase) displaces air or vacuum (assumed to be the wetting phase). Therefore, some independent estimate of S_{wi} is necessary to be able to predict the behavior of a gas-water system. Daigle et al. (2015) showed that the volume of clay-bound water in marine muds can be determined from porosity and fraction of clay-sized (<2 μm) grains. Since S_{wi} represents the amount of water remaining in the pore system at infinite capillary pressure, the amount of clay-bound water can be used as a reasonable proxy. Therefore we determined S_{wi} following Daigle et al. (2015) as

$$S_{wi} = \left(0.326 \pm 0.0220\right)f_c^{0.219 \pm 0.103} + \left(0.0262 \pm 0.00915\right)/\varphi, \tag{13}$$

where the reported errors are ±1 standard deviation. The Brooks-Corey capillary drainage curves with parameters determined from Equations 10–12 are shown in Figure 4 for $\varphi = 0.7$ (Figure 4a) and 0.4 (Figure 4b) and $f_c = 0.7$ and 0.2. Our approach differs from that of Leverett (1941) in that knowledge of permeability

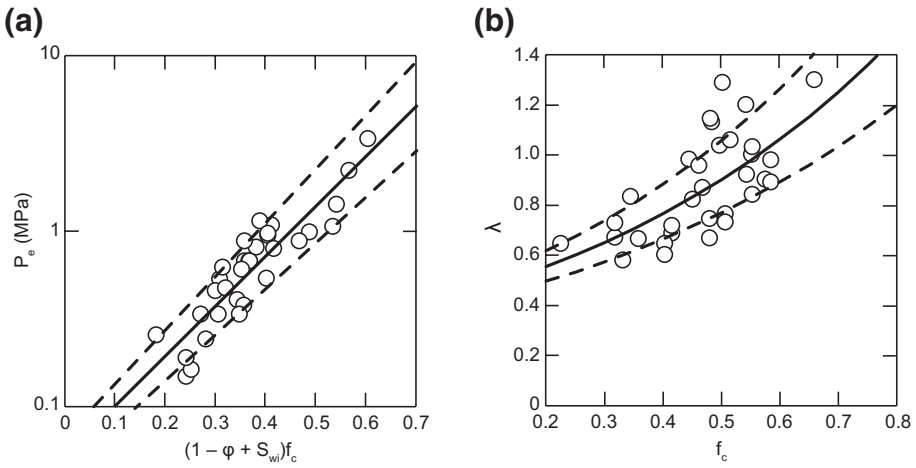

Figure 3. (a) Correlation for predicting entry pressure. (b) Correlation for predicting λ. Solid lines in both plots are best fit, while the dashed lines are ±1 standard deviation.

is not necessary. Indeed, formulating the capillary pressure curve in terms of porosity and clay-size fraction allows more direct facies-based prediction using empirical models that are specific to shallow marine sediments.

3.4. Fracture versus Flow

Gas will migrate by porous flow instead of initiating tensile fractures if it achieves the mobility threshold at a capillary pressure below the fracturing criterion given by Equation 2 and the intrinsic sediment permeability and gas-phase relative permeability are large enough to allow flow without additional pressure buildup. Based on the work of Schowalter (1979), we assumed a mobility threshold gas saturation of 10%, where the gas saturation $S_g = 1 - S_w$. If the fracturing criterion is achieved at gas saturations lower than this value, then tensile fracturing will occur before porous flow (Figure 5a). If the capillary pressure at 10% gas saturation is smaller than the fracture criterion (Figure 5b), this does not necessarily preclude tensile fracturing. At gas saturations greater than but very close to the mobility threshold, the relative

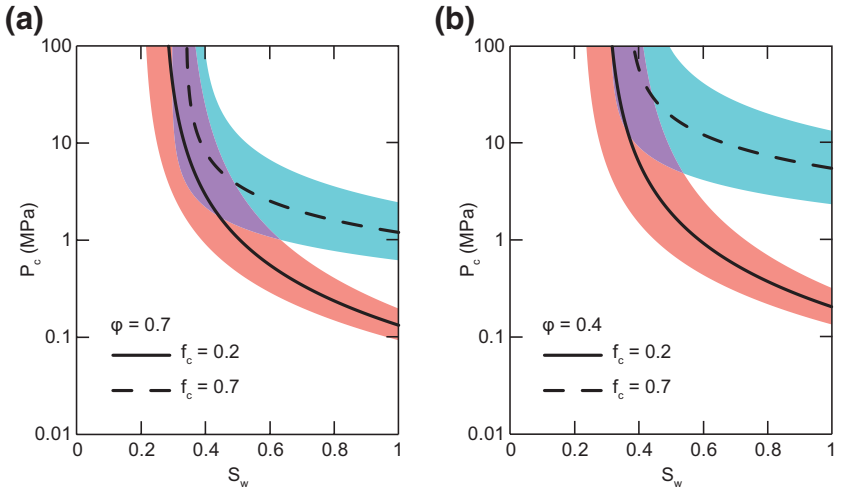

Figure 4. Predicted capillary drainage curves for porosities of 0.7 (a) and 0.4 (b) at clay fractions of 0.2 and 0.7. The shaded regions represent the overall uncertainty based on the uncertainties of the input parameters.

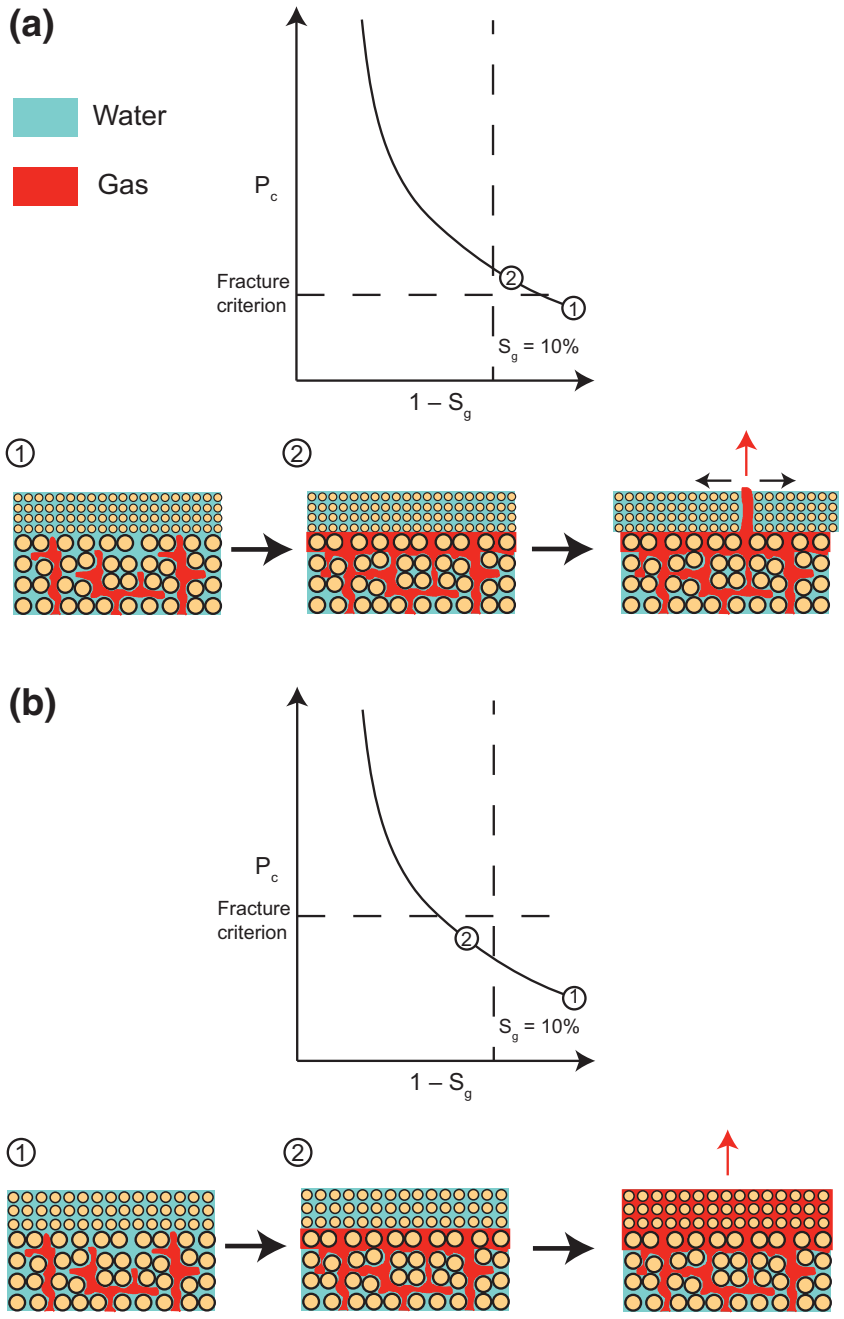

Figure 5. (a) Capillary pressure at the fracture criterion corresponding to a gas saturation smaller than the mobility threshold. At point 1, gas (red) starts accumulating in the sediment. This could be due to local microbial methanogenesis, hydrate dissociation, or buoyant migration of discrete bubbles from a deeper source. The gas continues accumulating to a gas saturation and capillary pressure represented by point 2. At this point, the fracture criterion is exceeded and the gas opens a tensile fracture, allowing buoyant migration. (b) Capillary pressure at the fracture criterion corresponding to a gas saturation larger than the mobility threshold. Gas starts accumulating (point 1) to a saturation and capillary pressure corresponding to point 2. Since this saturation is larger than the mobility threshold and the capillary pressure is smaller than the fracture criterion, the gas can move by porous flow.

permeability of the gas phase would be very low. If the rate of gas generation exceeds the rate of gas flow, gas can continue to accumulate and may reach the fracture criterion even in the presence of porous flow. This would be more likely in sediments with lower permeability, but understanding this process completely requires detailed models of multiphase flow, which are beyond the scope of the present work.

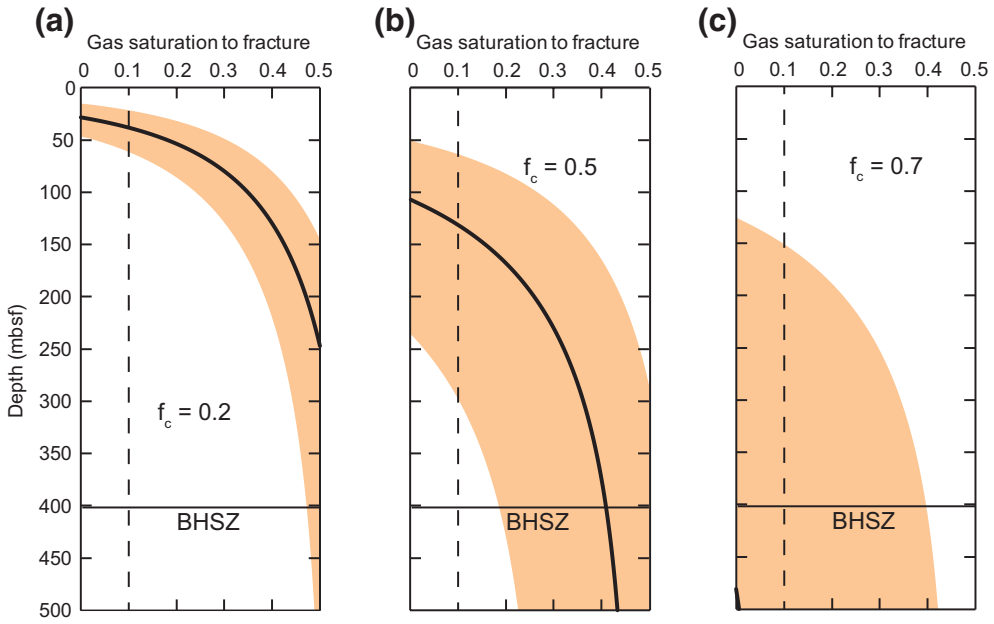

Figure 6. Gas saturation required to reach the fracture criterion in our generic passive margin sediments for clay fractions of 0.2 (a), 0.5 (b), and 0.7 (c). The solid black line represents the median prediction, while the shaded region shows the uncertainty. The vertical dashed line indicates the gas mobility threshold. Fracturing will happen whenever the solid black line is to the left of the vertical dashed line.

Note that using a 10% mobility threshold will give more conservative estimates of fracturing behavior than using the percolation threshold, which is considerably larger than 10% in shallow marine muds (Daigle et al., 2019). Future research should investigate gas mobility thresholds specific to marine muds, and how this threshold varies during burial.

4. Results

4.1. Generic Marine Hydrate System

We considered the tensile fracturing behavior of a generic marine hydrate system. The seafloor depth and temperature were 2,000 m and 3°C, and the geothermal gradient was 40°C/km. These values were selected to represent a deepwater, passive continental margin. The water density and salinity were 1,024 kg/m^3 and 3.5 wt% NaCl equivalent and the water-phase pressure was assumed hydrostatic. Based on the sI methane hydrate equilibrium temperature-pressure curve obtained from the CSMHYD program (Sloan, 1998), the base of the hydrate stability zone (BHSZ) was located at 403 mbsf.

Figure 6 shows the range of gas saturations necessary to form tensile fractures (±1 standard deviation), taking into account the uncertainties in the Brooks-Corey parameters and Hoek-Brown tensile strength estimate. In each panel of Figure 6, the mobility threshold is marked with a dashed vertical line. Tensile fracturing will be favored over porous flow wherever the gas saturation necessary for fracture (dark black line) is to the left of the mobility threshold line, and above the depth where the dark black line reaches the y-axis, any amount of gas will be sufficient to generate a fracture. For sediments with $f_c = 0.2$, fracturing occurs at gas saturations less than 10% shallower than 38 mbsf for the median case, indicating that gas accumulation in the shallowest 38 m of sediment will tend to result in tensile fracturing rather than porous flow (Figure 6a). As f_c increases, fracturing is favored over more of the hydrate stability zone. For $f_c = 0.5$, fracturing is possible in the median case shallower than 132 mbsf (Figure 6b), and for $f_c = 0.7$ fracturing is possible in the median case over the entire hydrate stability zone (Figure 6c). Increasing the clay-sized fraction of the sediment thus makes gas-driven tensile fracturing more likely and increases the depth interval over which fracturing is possible before reach-

ing the mobility threshold. Since the absolute permeability of marine muds decreases with increasing clay-sized fraction at constant porosity (Daigle & Screaton, 2015), higher clay-sized fraction will also decrease the rate of excess pore pressure dissipation, which would further promote tensile fracturing at gas saturations above the mobility threshold in the case of sufficiently rapid gas evolution from hydrate dissociation or an external source.

4.2. Fracturing Caused by Hydrate Dissociation at the BHSZ

While we have demonstrated the conditions that favor gas-driven tensile fracturing within the hydrate stability zone, a more pertinent question for hydrate-bearing sediments is the potential for gas-driven fracturing at the BHSZ, as this is where hydrate will first dissociate as a result of an increase in the steady-state temperature profile (Ruppel, 2011). Indeed, many locations around the world already have thick gas columns trapped beneath the BHSZ (Flemings et al., 2003; Hornbach et al., 2004; Tréhu et al., 2004), which raises the possibility that the sediments in these locations may already be near or at the conditions required for tensile failure.

We considered a generic passive margin setting in water depths ranging from 500 to 3,000 m. The seawater density and salinity and geothermal gradient were the same as those assumed in Section 4.1. For the temperature at the sea floor, we interpolated the temperature-depth data presented by Phrampus and Hornbach (2012) based on conductivity-temperature-depth (CTD) casts in the vicinity of the Blake Ridge outside the influence of the Gulf Stream. While these data are specific to Blake Ridge, Phrampus and Hornbach (2012) compared the data to similar data from the eastern Pacific Ocean and found agreement to within 1.5°C, suggesting that these data are representative of a generic sea floor temperature. Using the seafloor temperature, specified geothermal gradient, and hydrostatic pressure, we determined the depth of the BHSZ by comparing the in situ temperature with the equilibrium temperature-pressure data from CSMHYD (Figure 7a). No hydrate stability zone exists in the sediments at water depths shallower than 523 m, and this water depth represents the updip limit or feather edge of the hydrate stability zone, so called because thickness of the hydrate stability zone within the sediments decreases to zero at this water depth (McIver, 1982; Ruppel, 2011). At greater water depths, the hydrate stability zone thickens, reaching a thickness of 483 m at 3,000 m water depth.

Since the tensile strength of marine muds increases with depth, as does the minimum principal stress, greater amounts of gas are required to initiate tensile fractures at the BHSZ in deeper water. For sediments with $f_c = 0.2$, the median gas saturation necessary to fracture at the BHSZ is smaller than 10% only for water depths shallower than 560 m (Figure 7b), indicating that tensile failure of coarser-grained marine muds at the BHSZ is unlikely except right at the feather edge of the hydrate stability zone. As clay-sized fraction increases, fracturing at the BHSZ becomes easier. At $f_c = 0.5$, the median gas saturation required for fracturing at the BHSZ is less than 10% for water depths shallower than 670 m (Figure 7c), and 1,670 m for $f_c = 0.7$ (Figure 7d). Note that we are neglecting the effect, if any, that hydrate might have on tensile strength.

We also determined the minimum clay-sized fraction necessary for gas-driven tensile failure at the BHSZ, defined as the value of f_c that yields a median capillary pressure at 10% gas saturation equal to the median fracturing criterion. This value increases rapidly from zero to around 0.6 as water depth increases from 523 to 1,000 m, and increases only slightly with further increase in water depth. For a water depth of 3,000 m, the sediments at the BHSZ must have $f_c > 0.69$ for gas-driven tensile failure (Figure 7e). At the updip limit of the hydrate stability zone, fracturing is much easier. Our modeling suggests that fracturing will always occur, regardless of clay-sized fraction, at the feather edge and in water depths as deep as 540 m (Figure 7f). At greater water depths (up to 3,000 m), fracturing can always occur as long as f_c is large enough. We note here that our analysis is based on capillary pressure correlations developed using sediments with a minimum f_c of 0.2, so it is not clear whether our results are generalizable to sediments with less clay. However, Fauria and Rempel (2011) showed that gas can form tensile fractures in unconsolidated, coarse-grained sand (grain sizes on the order of mm), particularly at low effective stresses, so our predictions should hold in shallow sands.

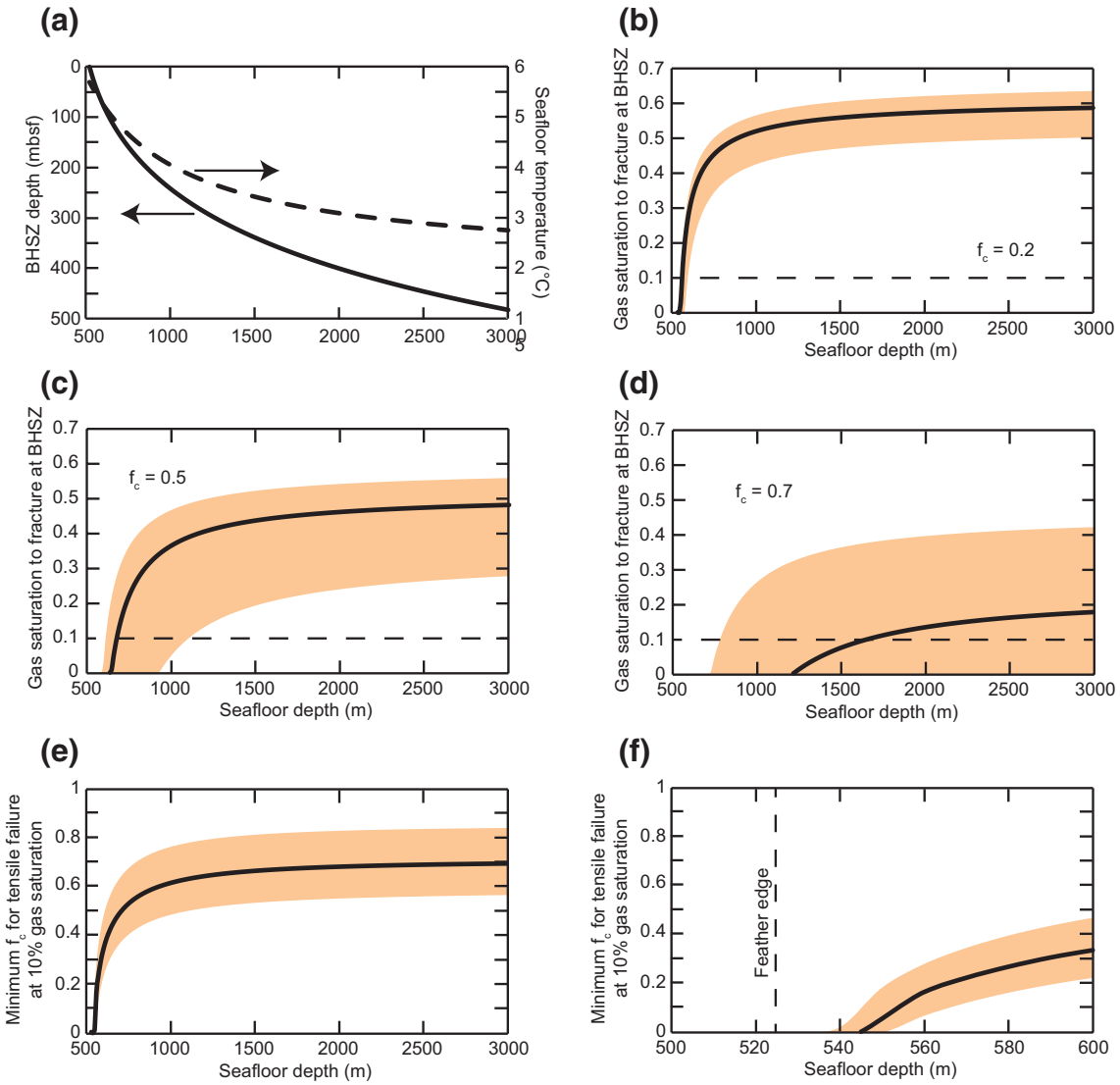

Figure 7. (a) Seafloor temperature and BHSZ depth as a function of water depth for our modeled case. Temperature based on data from Phrampus and Hornbach (2012). The arrows indicate that BHSZ depth (solid line) is plotted on the left-hand *y*-axis while seafloor temperature (dashed line) is plotted on the right-hand *y*-axis. (b–d) Critical gas saturations to cause fracturing at the BHSZ for clay fractions of 0.2, 0.5, and 0.7. The gas mobility threshold is marked with a dashed line. (e) Minimum clay fraction that will result in fracturing at the BHSZ at 10% gas saturation. (f) Close-up of (e) showing the vicinity of the feather edge (523 m seafloor depth; dashed line). Solid black lines in all plots represent the median prediction, while the shaded regions represent the uncertainty.

5. Discussion

5.1. How Much Hydrate Needs to Dissociate?

Gas-driven tensile fracturing is important to understand in the context of the global carbon cycle. Fractures that breach the sea floor and allow venting of gas from below the BHSZ provide important nutrients for chemosynthetic communities at the sea floor (e.g., Torres et al., 2002; Tryon et al., 2002). Over larger spatial and time scales, gas hydrate can act as a capacitor in the global carbon cycle, holding carbon for long periods of time and releasing it in response to external perturbations (Dickens, 2003). The factors governing the evolution of gas from hydrates are well understood, but the fate of that gas, including what determines its rate of transfer to the ocean, is not. Gas venting at the seafloor inferred to emanate from dissociating hydrates is observed at many locations worldwide, in response to both postglacial isostatic rebound and ocean temperature changes and anthropogenic warming (Ruppel & Kessler, 2017). This venting may result from a combination of dissociation-derived gas accumulation and migration of gas from depth and accumulation at the

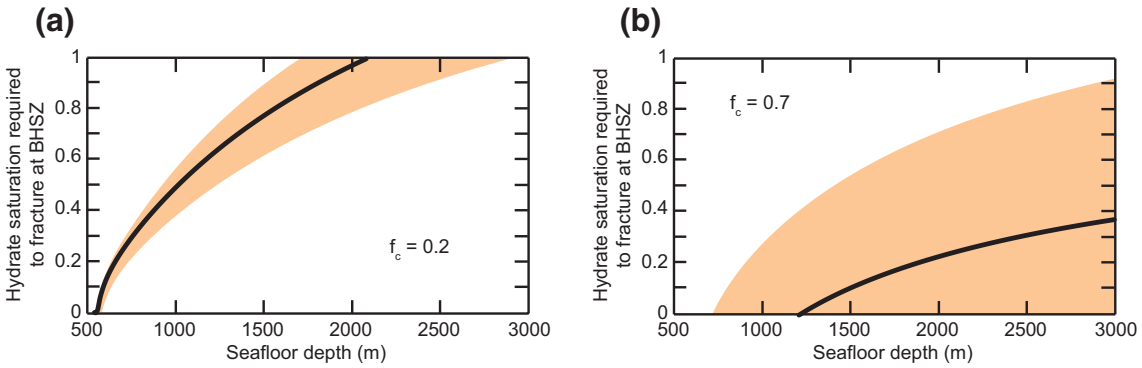

Figure 8. Initial hydrate saturation that would need to dissociate to cause fracturing at the BHSZ as a function of water depth for clay fractions of 0.2 (a) and 0.7 (b). The solid black lines represent the median prediction, while the shaded regions represent the uncertainty.

BHSZ (e.g., Daigle et al., 2011; Plaza-Faverola & Keiding, 2019). Understanding the role of hydrate-derived gas in this process is central to predicting how hydrate systems respond to external perturbations.

The question arises, then, about how much hydrate needs to dissociate to generate the gas volumes required to initiate tensile fractures. At standard temperature and pressure, the molar volume of methane gas is roughly 164 times that of sI methane hydrate (Collett et al., 2015), but at in situ conditions, this ratio is much smaller. For instance, using the modified Lee-Kesler equation of state for methane described by Duan et al. (1992), at the in situ pressure and temperature in the vicinity of the BHSZ at Ocean Drilling Program (ODP) Site 997 on Blake Ridge (roughly 34.5 MPa and 21°C [C. Ruppel, 1997; Flemings et al., 2003]), the molar volume of methane gas is only about 0.51 times that of sI methane hydrate. At these conditions, the initial hydrate saturation would be nearly twice the corresponding gas saturation following dissociation. In porous media, the situation is slightly more complicated since the capillary pressure of the gas phase must also be considered.

If porosity does not change upon hydrate dissociation, the hydrate saturation S_h necessary to yield a particular gas saturation S_g is given by

$$S_h = S_g \frac{V_{m,h}}{V_{m,g}}, \tag{14}$$

where $V_{m,h}$ and $V_{m,g}$ are the molar volumes of hydrate and gas, respectively. We considered the hydrate saturation necessary to yield the gas saturation required to generate tensile fracturing at the BHSZ. $V_{m,g}$ was calculated using the equation of state of Duan et al. (1992) at the in situ temperature and a gas pressure equal to hydrostatic pressure plus the capillary pressure corresponding to the critical gas saturation for fracture. $V_{m,h}$ was assumed constant and was determined as 1.29×10^{-4} m^3/mol based on a molar mass for sI hydrate ($CH_4 \cdot 5.75H_2O$) of 0.1192 kg/mol and a hydrate bulk density of 925 kg/m^3 (Waite et al., 2009).

Figure 8 shows the hydrate saturations required to generate fractures at $f_c = 0.2$ and $f_c = 0.7$. Since capillary pressures are lower when less clay is present, more gas and correspondingly more dissociated hydrate are required to generate fractures. In water depths greater than 1,000 m when $f_c = 0.2$, a hydrate saturation of greater than 50% would need to dissociate to generate a sufficient amount of gas to cause tensile fractures (Figure 8a). However, the larger capillary pressures in sediments with more clay will reduce the molar volume of methane gas, which means that more hydrate will need to dissociate to generate the required gas saturation. This explains the wide range of required hydrate saturations at $f_c = 0.7$ (Figure 8b). Hydrate saturations in marine muds rarely exceed 10% except in localized cases (Boswell & Collett, 2006), and so it appears unlikely that hydrate dissociation at the BHSZ in deepwater settings (water depths greater than about 1,500 m) would lead to gas-driven tensile fracturing, except in cases of localized, high-saturation accumulations of hydrate. On the other hand, near the feather edge, any amount of dissociated hydrate can lead to tensile fracturing.

This analysis assumes that any excess water-phase pressure that develops following hydrate dissociation dissipates rapidly. If excess water-phase pressure is retained at least partially for some time, this will reduce the molar volume of methane gas and further increase the amount of hydrate needed to generate gas and achieve the capillary pressure necessary for fracture. Likewise, we ignore the endothermic nature of hydrate dissociation (Waite et al., 2009), which would perturb the in situ temperature.

5.2. Venting at the Feather Edge

Seafloor methane venting has been observed on many continental margins close to the feather edge where the BHSZ outcrops at the seafloor and may be related to changes in water temperature or depth on time scales ranging from seasonal to glacial-interglacial, including since the onset of the Industrial Age (Ruppel & Kessler, 2017). Changes in ocean temperature will tend to affect hydrates nearest the seafloor first, and, in this context, the observed methane venting near the feather edge is not surprising (e.g., Phrampus & Hornbach, 2012), although it may be possible for gas derived from dissociation downdip of the feather edge or from a deep nonhydrate source to migrate updip (e.g., Darnell & Flemings, 2015). Our calculations indicate that any sediment, regardless of clay-sized fraction, is susceptible to tensile failure at the feather edge, and that any amount of hydrate dissociation will preferentially form fractures as the evolved gas vents to the water column. Observable seafloor gas venting at the feather edge does not require very much hydrate to dissociate because of gas expansion. At the pressure and temperature we considered at the feather edge (5.3 MPa, 5.7°C), 1 mol of methane gas occupies 3.0 times the volume of 1 mol of methane hydrate. With a seafloor sediment porosity of 0.775 based on the Kominz et al. (2011) model, dissociation of 1% hydrate saturation would produce 23.5 L of methane gas per m^3 of sediment. Widespread observations of seafloor methane bubble discharge from discrete vents near the feather edge (Berndt et al., 2014; Ketzer et al., 2019; Sarkar et al., 2012; Skarke et al., 2014) are consistent with our predictions and require only small amounts of hydrate dissociation to appear (e.g., Stranne et al., 2017). However, we caution that venting near the feather edge is not necessarily an indication of hydrate dissociation, since microbial methanogenesis in sediments outside the hydrate stability zone can still produce gas that can cause fracturing and venting (e.g., Naudts et al., 2009; Skarke et al., 2014).

5.3. The Role of Lithologic Heterogeneity

The predicted critical gas saturations for tensile failure shown in Figures 6–8 all assume a uniform lithology (i.e., constant f_c) between the BHSZ and seafloor. The marine subsurface is more complicated than this, often exhibiting mixtures of lithologies (clay-rich, silty, sandy) in vertical and lateral successions. At a given porosity, sediments with less clay will be less prone to fracture, and it is conceivable that a propagating fracture may be arrested upon intersecting a coarser-grained layer since the capillary pressure will be lower in the coarser-grained layer. A similar fracture-arresting phenomenon due to contrasts in mechanical properties is well known in lithified sediments, for example, hydrocarbon reservoirs (e.g., Rijken & Cooke, 2001), and may provide a migration pathway for gas to form hydrates in coarser-grained layers within the hydrate stability zone (Cook et al., 2008). Although the expansion of gas as it rises buoyantly will tend to promote a fracture's propagation once it initiates, extreme cases like chimneys that reach from the BHSZ to the seafloor are likely to form only in relatively homogeneous sediments.

6. Conclusions

We demonstrated that gas-driven tensile fracturing is generally favored in the shallowest sediments, but fracturing is possible in deeper sediments as well as clay content increases. With $f_c = 0.2$, fracturing is only favored in the shallowest 38 m of sediment, but fracturing may be possible to a depth of 132 mbsf when $f_c = 0.5$ and to a depth of nearly 500 mbsf when $f_c = 0.7$. This means that the potential for gas-driven tensile fracturing caused by dissociation of hydrate at the BHSZ is greatest in shallower water, where the BHSZ is closer to the seafloor.

Dissociating hydrate at the BHSZ can be a source of gas that can in turn cause tensile failure. We found that in clay-poor sediments ($f_c = 0.2$), more than 20% initial hydrate saturation would need to dissociate to generate gas-driven tensile fractures for all but the very shallowest water depths considered (<600 m). However, when the sediments have more clay, much less dissociated hydrate is necessary. At $f_c = 0.7$, any amount of dissociated hydrate can generate tensile fractures at the BHSZ in water depths as great as 1,000 m. Fracturing potential is greatest near the feather edge of the hydrate stability zone: any amount of gas can generate fractures, regardless of the clay-sized fraction. This ease of fracturing combines with significant gas expansion relative to original hydrate volume (roughly a factor of 3) to allow seafloor gas venting near the feather edge with even minor amounts of hydrate dissociation.

Our work overall has shown the conditions under which gas-driven tensile fracturing may occur. The results presented here were based on simplifying assumptions and an idealized case of a passive continental margin, and predicting fracturing behavior at specific sites around the world would require more detailed knowledge of many different factors. However, the general conclusion that gas-driven tensile failure is probably a common occurrence near the seafloor and does not require much gas is consistent with previous work (e.g., Stranne et al., 2017) and it is important to consider in future studies of the source and fate of gas in the shallow marine subsurface.

Data Availability Statement

The data on which this article is based are available at https://doi.org/10.5281/zenodo.4253698.

Acknowledgments
This work was supported by the University of Texas at Austin, and the Laboratory Directed Research and Development program at Sandia National Laboratories. Sandia National Laboratories is a multimission laboratory managed and operated by National Technology and Engineering Solutions of Sandia, LLC., a wholly owned subsidiary of Honeywell International, Inc., for the U.S. Department of Energy's National Nuclear Security Administration under contract DE-NA-0003525. A. Cook was supported by NSF Award 1752882. Constructive comments from Christian Stranne, Associate Editor Brandon Dugan, and an anonymous reviewer helped strengthen this paper.

References

Algar, C. K., & Boudreau, B. P. (2010). Stability of bubbles in a linear elastic medium: Implications for bubble growth in marine sediments. *Journal of Geophysical Research*, *115*(F3), F03012. https://doi.org/10.1029/2009JF001312

Algar, C. K., Boudreau, B. P., & Barry, M. A. (2011). Release of multiple bubbles from cohesive sediments. *Geophysical Research Letters*, *38*, L08606. https://doi.org/10.1029/2011GL046870

Archer, D., Buffett, B., & Brovkin, V. (2009). Ocean methane hydrates as a slow tipping point in the global climate cycle. *Proceedings of the National Academy of Science of the United States of America*, *106*(49), 20596–20601. https://doi.org/10.1073/pnas.0800885105

Barry, M. A., Boudreau, B. P., Johnson, B. D., & Reed, A. H. (2010). First-order description of the mechanical fracture behavior of fine-grained surficial marine sediments during gas bubble growth. *Journal of Geophysical Research*, *115*(F4), F04029. https://doi.org/10.1029/2010JF001833

Bear, J. (1972). *Dynamics of fluids in porous media*. New York, NY: Elsevier.

Berndt, C., Feseker, T., Treude, T., Krastel, S., Liebetrau, V., Niemann, H., et al. (2014). Temporal constraints on hydrate-controlled methane seepage off Svalbard. *Science*, *343*(6168), 284–287. https://doi.org/10.1126/science.1246298

Best, A. I., Richardson, M. D., Boudreau, B. P., Judd, A. G., Leifer, I., Lyons, A. P., et al. (2006). Shallow seabed methane gas could pose coastal hazard. *EOS*, *87*(22), 213–217. https://doi.org/10.1029/2006EO220001

Bihani, A., & Daigle, H. (2019). On the role of spatially correlated heterogeneity in determining mudrock sealing capacity for CO_2 sequestration. *Marine and Petroleum Geology*, *106*, 116–127. https://doi.org/10.1016/j.marpetgeo.2019.04.038

Bishop, A. W. (1959). The principle of effective stress. *Teknisk Ukeblad*, *39*, 859–863.

Blunt, M. J. (2017). *Multiphase flow in permeable media*. Cambridge, UK: Cambridge University Press.

Boehm, A., & Moore, J. C. (2002). Fluidized sandstone intrusions as an indicator of Paleostress orientation, Santa Cruz, California. *Geofluids*, *2*(2), 147–161. https://doi.org/10.1046/j.1468-8123.2002.00026.x

Boswell, R., & Collett, T. S. (2006). The gas hydrates resource pyramid. *Fire in the Ice*, *6*(3), 5–7.

Boswell, R., & Collett, T. S. (2011). Current perspectives on gas hydrate resources. *Energy and Environmental Science*, *4*, 1206–1215. https://doi.org/10.1039/C0EE00203H

Boudreau, B. P. (2012). The physics of bubbles in surficial, soft, cohesive sediments. *Marine and Petroleum Geology*, *38*(1), 1–18. https://doi.org/10.1016/j.marpetgeo.2012.07.002

Boudreau, B. P., Algar, C., Johnson, B. D., Croudace, I., Reed, A., Furukawa, Y., et al. (2005). Bubble growth and rise in soft sediments. *Geology*, *33*(6), 517–520. https://doi.org/10.1130/G21259.1

Brooks, R. H., & Corey, A. T. (1964). *Hydraulic properties of porous media* (Hydrology Paper 3). Fort Collins, CO: Colorado State University.

Chatzis, I., & Dullien, F. A. L. (1977). Modelling pore structure by 2-D and 3-D networks with application to sandstones. *Journal of Canadian Petroleum Technology*, *16*(1), 97–108. https://doi.org/10.2118/77-01-09

Choi, J.-H., Seol, Y., Boswell, R., & Juanes, R. (2011). X-ray computed-tomography imaging of gas migration in water-saturated sediments: From capillary invasion to conduit opening. *Geophysical Research Letters*, *38*(17), L17310. https://doi.org/10.1029/2011GL048513

Clennell, M. B., Hovland, M., Booth, J. S., Henry, P., & Winters, W. J. (1999). Formation of natural gas hydrates in marine sediments 1. Conceptual model of gas hydrate growth conditioned by host sediment properties. *Journal of Geophysical Research*, *104*(B10), 22985–23003. https://doi.org/10.1029/1999JB900175

Collett, T., Bahk, J., Baker, R., Boswell, R., Divins, D., Frye, M., et al. (2015). Methane hydrates in nature—Current knowledge and challenges. *Journal of Chemical and Engineering Data*, *60*(2), 319–329. https://doi.org/10.1021/je500604h

Cook, A. E., & Goldberg, D. (2008). Extent of gas hydrate filled fracture planes: Implications for in situ methanogenesis and resource potential. *Geophysical Research Letters*, *35*(15), L15302. https://doi.org/10.1029/2008GL034587

Cook, A. E., Goldberg, D., & Kleinberg, R. L. (2008). Fracture-controlled gas hydrate systems in the northern Gulf of Mexico. *Marine and Petroleum Geology*, *25*, 932–941. https://doi.org/10.1026/j.marpetgeo.2008.01.013

Cook, A. E., Goldberg, D. S., & Malinverno, A. (2014). Natural gas hydrates occupying fractures: A focus on non-vent sites on the Indian continental margin and the northern Gulf of Mexico. *Marine and Petroleum Geology*, *58*(A), 278–291. https://doi.org/10.1016/j.marpetgeo.2014.04.013

Coussy, O. (2004). *Poromechanics*. Chichester, UK: John Wiley & Sons.

Coussy, O. (2007). Revisiting the constitutive equations of unsaturated porous solids using a Lagrangian saturation concept. *International Journal for Numerical and Analytical Methods in Geomechanics*, *31*, 1675–1694. https://doi.org/10.1002/nag.613

Daigle, H., Bangs, N. L., & Dugan, B. (2011). Transient hydraulic fracturing and gas release in methane hydrate settings: A case study from southern Hydrate Ridge. *Geochemistry, Geophysics, Geosystems*, *12*(12), Q12022. https://doi.org/10.1029/2011GC003841

Daigle, H., & Dugan, B. (2010a). Effects of multiphase methane supply on hydrate accumulation and fracture generation. *Geophysical Research Letters*, *37*(20), L20301. https://doi.org/10.1029/2010GL044970

Daigle, H., & Dugan, B. (2010b). Origin and evolution of fracture-hosted methane hydrate deposits. *Journal of Geophysical Research*, *115*(B11), B11103. https://doi.org/10.1029/2010JB007492

Daigle, H., & Dugan, B. (2011). Capillary controls on methane hydrate distribution and fracturing in advective systems. *Geochemistry, Geophysics, Geosystems*, *12*(1), Q01003. https://doi.org/10.1029/2010GC003392

Daigle, H., & Dugan, B. (2014). Data report: Permeability, consolidation, stress state, and pore system characteristics of sediments from Sites C0011, C0012, and C0018 of the Nankai Trough. In Proceedings of the Integrated Ocean Drilling Program (Vol. *333*, pp. 1–23). https://doi.org/10.2204/iodp.proc.333.201.2014

Daigle, H., Ghanbarian, B., Henry, P., & Conin, M. (2015). Universal scaling of the formation factor in clays: Example from the Nankai Trough. *Journal of Geophysical Research Solid Earth*, *120*(11), 7361–7375. https://doi.org/10.1002/2015JB012262

Daigle, H., Reece, J. S., & Flemings, P. B. (2019). Evolution of the percolation threshold in muds and mudrocks during burial. *Geophysical Research Letters*, *46*(14), 8064–8073. https://doi.org/10.1029/2019GL083723

Daigle, H., & Screaton, E. J. (2015). Predicting the permeability of sediments entering subduction zones. *Geophysical Research Letters*, *42*(13), 5219–5226. https://doi.org/10.1002/2015GL064542

Darnell, K. N., & Flemings, P. B. (2015). Transient seafloor venting on continental slopes from warming-induced methane hydrate dissociation. *Geophysical Research Letters*, *42*(24), 10765–10772. https://doi.org/10.1002/2015GL067012

Diaz, C. E., Chatzis, I., & Dullien, F. A. L. (1987). Simulation of capillary pressure curves using bond correlated site percolation on a simple cubic network. *Transport in Porous Media*, *2*(3), 215–240. https://doi.org/10.1007/BF00165783

Dickens, G. R. (2003). Rethinking the global carbon cycle with a large, dynamic and microbially mediated gas hydrate capacitor. *Earth and Planetary Science Letters*, *213*(3–4), 169–183. https://doi.org/10.1016/S0012-821X(03)00325-X

Duan, Z., Møller, N., & Weare, J. H. (1992). An equation of state for the CH_4-CO_2-H_2O system: I. Pure systems from 0 to 1000°C and 0 to 8000 bar. *Geochimica et Cosmochimica Acta*, *56*(7), 2605–2617. https://doi.org/10.1016/0016-7037(92)90347-L

Dugan, B., & Germaine, J. T. (2009). Data report: Strength characteristics of sediments from IODP Expedition 308, Sites U1322 and U1324. In Proceedings of the Integrated Ocean Drilling Program (Vol. *308*, pp. 1–13). https://doi.org/10.2204/iodp.proc.308.210.2009

Eaton, B. A. (1969). Fracture gradient prediction and its application in oilfield operations. *Journal of Petroleum Technology*, *21*(10), 1353–1360. https://doi.org/10.2118/2163-PA

Ewing, R. P., & Gupta, S. C. (1993). Modeling percolation properties of random media using a domain network. *Water Resources Research*, *29*(9), 3169–3178. https://doi.org/10.1029/93WR01496

Fauria, K. E., & Rempel, A. W. (2011). Gas invasion into water-saturated, unconsolidated porous media: Implications for gas hydrate reservoirs. *Earth and Planetary Science Letters*, *312*(1–2), 188–193. https://doi.org/10.1016/j.epsl.2011.09.042

Flemings, P. B., Liu, X., & Winters, W. J. (2003). Critical pressure and multiphase flow in Blake Ridge gas hydrates. *Geology*, *31*(12), 1057–1060. https://doi.org/10.1130/g19863.1

Ginsburg, G. D., & Soloviev, V. A. (1997). Methane migration within the submarine gas-hydrate stability zone under deep-water conditions. *Marine Geology*, *137*(1–2), 49–57. https://doi.org/10.1016/S0025-3227(96)00078-3

Griffith, A. A. (1921). The phenomena of rupture and flow in solids. *Philosophical Transactions of the Royal Society A*, *221*, 582–593. https://doi.org/10.1098/rsta.1921.0006

Hamilton, E. L. (1979). V_p/V_s and Poisson's ratios in marine sediments and rocks. *Journal of the Acoustical Society of America*, *66*(4), 1093–1101. https://doi.org/10.1121/1.383344

Henry, P., Thomas, M., & Clennell, M. B. (1999). Formation of natural gas hydrates in marine sediments 2. Thermodynamic calculations of stability conditions in porous sediments. *Journal of Geophysical Research*, *104*(B10), 23005–23022. https://doi.org/10.1029/1999JB900167

Hildenbrand, A., Schlömer, S., & Krooss, B. M. (2002). Gas breakthrough experiments on fine-grained sedimentary rocks. *Geofluids*, *2*(1), 3–23. https://doi.org/10.1046/j.1468-8123.2002.00031.x

Hildenbrand, A., Schlömer, S., Krooss, B. M., & Littke, R. (2004). Gas breakthrough experiments on politic rocks: Comparative study with N_2, CO_2 and CH_4. *Geofluids*, *4*(1), 61–80. https://doi.org/10.1111/j.1468-8123.2004.00073.x

Hirasaki, G. J. (1991). Wettability: Fundamentals and surface forces. *SPE Formation Evaluation*, *6*(2), 217–226. https://doi.org/10.2118/17367-PA

Hoek, E. (2006). *Practical rock engineering*. Retrieved from https://www.rocscience.com/assets/resources/learning/hoek/Practical-Rock-Engineering-Full-Text.pdf

Hoek, E., & Brown, E. T. (1997). Practical estimates of rock mass strength. *International Journal of Rock Mechanics and Mining Sciences*, *34*(8), 1165–1186. https://doi.org/10.1016/S1365-1609(97)80069-X

Holtzman, R., & Juanes, R. (2011). Thermodynamic and hydrodynamic constraints on overpressure caused by hydrate dissociation: A pore-scale model. *Geophysical Research Letters*, *38*(14), L14308. https://doi.org/10.1029/2011GL047937

Hornbach, M. J., Saffer, D. M., & Holbrook, W. S. (2004). Critically pressured free-gas reservoirs below gas-hydrate provinces. *Nature*, *427*, 142–144. https://doi.org/10.1038/nature02172

Hustoft, S., Bünz, S., Mienert, J., & Chand, S. (2009). Gas hydrate reservoir and active methane-venting province in sediments on < 20 Ma young oceanic crust in the Fram Strait, offshore NW-Svalbard. *Earth and Planetary Science Letters*, *284*(1–2), 12–24. https://doi.org/10.1016/j.epsl.2009.03.038.

Ingram, G. M., & Urai, J. L. (1999). Top-seal leakage through faults and fractures: The role of mudrock properties. In A. C. Aplin, A. J. Fleet, & J. H. S. Macquaker (Eds.), Muds and mudstones: Physical and fluid flow properties, Geological Society, London, Special Publications (Vol. *158*, pp. 125–135). London: The Geological Society of London. https://doi.org/10.1144/GSL.SP.1999.158.01.10

Jain, A. K., & Juanes, R. (2009). Preferential mode of gas invasion in sediments: Grain-scale mechanistic model of coupled multiphase fluid flow and sediment mechanics. *Journal of Geophysical Research*, *114*(B8), B08101. https://doi.org/10.1029/2008JB006002

James, R. H., Bousquet, P., Bussmann, I., Haeckel, M., Kipfer, R., Leifer, I., et al. (2016). Effects of climate change on methane emissions from seafloor sediments in the Arctic Ocean: A review. *Limnology and Oceanography*, *61*, S283–S299. https://doi.org/10.1002/lno.10307

Jin, Z., Johnson, S. E., & Cook, A. E. (2015). Crack extension induced by dissociation of fracture-hosted methane gas hydrate. *Geophysical Research Letters*, *42*(20), 8522–8529. https://doi.org/10.1002/2015GL066060

Johnson, B. D., Barry, M. A., Boudreau, B. P., Jumars, P. A., & Dorgan, K. M. (2012). In situ tensile fracture toughness of surficial cohesive marine sediments. *Geo-Marine Letters*, *32*(1), 39–48. https://doi.org/10.1007/s00367-011-0243-1

Johnson, B. D., Boudreau, B. P., Gardiner, B. S., & Maass, R. (2002). Mechanical response of sediments to bubble growth. *Marine Geology*, *187*(3–4), 347–363. https://doi.org/10.1016/s0025-3227(02)00383-3

Ketzer, M., Praeg, D., Pivel, M. A. G., Augustin, A. H., Rodrigues, L. F., Viana, A. R., & Cupertino, J. A. (2019). Gas seeps at the edge of the gas hydrate stability zone on Brazil's continental margin. *Geosciences*, *9*, 193. https://doi.org/10.3390/geosciences9050193

Kominz, M. A., Patterson, K., & Odette, D. (2011). Lithology dependence of porosity in slope and deep marine sediments. *Journal of Sedimentary Research*, *81*(10), 730–742. https://doi.org/10.2110/jsr.2011.60

Larson, R. G., & Morrow, N. R. (1981). Effects of sample size on capillary pressures in porous media. *Powder Technology*, *30*(2), 123–138. https://doi.org/10.1016/0032-5910(81)80005-8

Lenormand, R., Zarcone, C., & Sarr, A. (1983). Mechanisms of the displacement of one fluid by another in a network of capillary ducts. *Journal of Fluid Mechanics*, *135*, 337–353. https://doi.org/10.1017/S0022112083003110

Leverett, M. C. (1941). Capillary behavior in porous solids. *Transactions of the AIME*, *142*(1), 152–169. https://doi.org/10.2118/941152-G

Liu, X., & Flemings, P. B. (2007). Dynamic multiphase flow model of hydrate formation in marine sediments. *Journal of Geophysical Research*, *112*(B3), B03101. https://doi.org/10.1029/2005JB004227

Maslin, M., Owen, M., Betts, R., Day, S., Dunkley Jones, T., & Ridgwell, A. (2010). Gas hydrates: Past and future geohazard? *Philosophical Transactions of the Royal Society A*, *368*(1919), 2369–2393. https://doi.org/10.1098/rsta.2010.0065

McCave, I. N., & Hall, I. R. (2006). Size sorting in marine muds: Processes, pitfalls, and prospects for paleoflow-speed proxies. *Geochemistry, Geophysics, Geosystems*, *7*(10), Q10N05. https://doi.org/10.1029/2006GC001284

McCave, I. N., Manighetti, B., & Robinson, S. G. (1995). Sortable silt and fine sediment size/composition slicing: Parameters for paleocurrent speed and paleoceanography. *Paleoceanography*, *10*(3), 593–610. https://doi.org/10.1027/94PA03039

McIver, R. D. (1982). Role of naturally occurring gas hydrates in sediment transport. *AAPG Bulletin*, *66*(6), 789–792. https://doi.org/10.1306/03b5a318-16d1-11d7-8645000102c1865d

Moses, G. G., Rao, S. N., & Rao, P. N. (2003). Undrained strength behaviour of a cemented marine clay under monotonic and cyclic loading. *Ocean Engineering*, *30*(14), 1765–1789. https://doi.org/10.1016/S0029-8018(03)00018-0

Natzeband, G. L., Hübscher, C. P., Gajewski, D., Grobys, J. W. G., & Bialas, J. (2005). Seismic velocities from the Yaquina forearc basin off Peru: Evidence for free gas within the gas hydrate stability zone. *International Journal of Earth Sciences*, *94*(3), 420–432. https://doi.org/10.1007/s00531-005-0483-2

Naudts, L., De Batist, M., Greinert, J., & Artemov, Y. (2009). Geo- and hydro-acoustic manifestations of shallow gas and gas seeps in the Dnepr paleodelta, northwestern Black Sea. *The Leading Edge*, *28*(9), 1030–1040. https://doi.org/10.1190/1.3236372

Nimblett, J., & Ruppel, C. (2003). Permeability evolution during the formation of gas hydrates in marine sediments. *Journal of Geophysical Research*, *108*(B9), 2420. https://doi.org/10.1029/2001JB001650

Nuth, M., & Laloui, L. (2008). Effective stress concept in unsaturated soils: Clarification and validation of a unified framework. *International Journal for Numerical and Analytical Methods in Geomechanics*, *32*(7), 771–801. https://doi.org/10.1002/nag.645

Phrampus, B. J., & Hornbach, M. J. (2012). Recent changes to the Gulf Stream causing widespread gas hydrate destabilization. *Nature*, *490*, 527–530. https://doi.org/10.1038/nature11528

Plaza-Faverola, A., & Keiding, M. (2019). Correlation between tectonic stress regimes and methane seepage on the western Svalbard margin. *Solid Earth*, *10*, 79–94. https://doi.org/10.5194/se-10-79-2019

Purcell, W. R. (1949). Capillary pressures – Their measurement using mercury and the calculation of permeability therefrom. *Journal of Petroleum Technology*, *1*(2), 39–48. https://doi.org/10.2118/949039-g

Reece, J. S., Flemings, P. B., & Germaine, J. T. (2013). Data report: Permeability, compressibility, and microstructure of resedimented mudstone from IODP Expedition 322, Site C0011. In Proceedings of the Integrated Ocean Drilling Program (Vol. *322*, pp. 1–26). https://doi.org/10.2204/iodp.proc.322.205.2013

Rees, E. V. L., Priest, J. A., & Clayton, C. R. I. (2011). Thermodynamic and hydrodynamic constraints on overpressure caused by hydrate dissociation: A pore-scale model. *Marine and Petroleum Geology*, *28*(7), 1283–1293. https://doi.org/10.1016/j.marpetgeo.2011.03.015

Rempel, A. W. (2011). A model for the diffusive growth of hydrate saturation anomalies in layered sediments. *Journal of Geophysical Research*, *116*(B10), B10105. https://doi.org/10.1029/2011JB008484

Reynolds, J. M. (1997). *An introduction to applied and environmental geophysics*. Chichester, UK: John Wiley.

Rijken, P., & Cooke, M. L. (2001). Role of shale thickness on vertical connectivity of fractures: Application of crack-bridging theory to the Austin Chalk, Texas. *Tectonophysics*, *337*(1–2), 117–133. https://doi.org/10.1016/S0040-1951(01)00107-X

Ruppel, C. (1997). Anomalously cold temperatures observed at the base of the gas hydrate stability zone on the U.S. Atlantic passive margin. *Geology*, *25*(8), 699–702. https://doi.org/10.1130/0091-7613(1997)025%3C0699:ACTOAT%3E2.3.CO;2

Ruppel, C. D. (2011). Methane hydrates and contemporary climate change. *Nature Education and Knowledge*, *3*(10), 29.

Ruppel, C. D., & Kessler, J. D. (2017). The interaction of climate change and methane hydrates. *Reviews of Geophysics*, *55*(1), 126–168. https://doi.org/10.1002/2016RG000534

Russel, W. B. (1980). Review of the role of colloidal forces in the rheology of suspensions. *Journal of Rheology*, *24*, 287–317. https://doi.org/10.1122/1.549564

Sahimi, M. (2011). *Flow and transport in porous media and fractured rock* (2nd ed.). Weinheim, Germany: Wiley-VCH.

Sarkar, S., Berndt, C., Minshull, T. A., Westbrook, G. K., Klaeschen, D., Masson, D. G., et al. (2012). Seismic evidence for shallow gas-escape features associated with a retreating gas hydrate zone offshore west Svalbard. *Journal of Geophysical Research*, *117*(B9), B09102. https://doi.org/10.1029/2011JB009126

Sassen, R., Losh, S. L., Cathles, L., Roberts, H. H., Whelan, J. K., Milkov, A. V., et al. (2001). Massive vein-filling gas hydrate: Relation to ongoing gas migration from the deep subsurface in the Gulf of Mexico. *Marine and Petroleum Geology*, *18*(5), 551–560. https://doi.org/10.1016/S0264-8172(01)00014-9

Sawyer, D. E., Jacoby, R., Flemings, P., & Germaine, J. T. (2008). Data report: Particle size analysis of sediments in the Ursa Basin, IODP Expedition 308 sites U1324 and U1322, northern Gulf of Mexico. In Proceedings of the Integrated Ocean Drilling Program (Vol. *308*, pp. 1–20). https://doi.org/10.2204/iodp.proc.308.205.2008

Schneider, J. (2011). *Compression and permeability behavior of natural mudstones* (Doctoral dissertation). Retrieved from Texas Scholar Works: https://repositories.lib.utexas.edu/handle/2152/ETD-UT-2011-12-4730. Austin, TX: University of Texas at Austin.

Schowalter, T. T. (1979). Mechanics of secondary hydrocarbon migration and entrapment. *AAPG Bulletin*, *63*(5), 723–760. https://doi.org/10.1306/2f9182ca-16ce-11d7-8645000102c1865d

Shin, H., & Santamarina, J. C. (2010). Fluid-driven fractures in uncemented sediments: Underlying particle-level processes. *Earth and Planetary Science Letters*, *299*, 180–189. https://doi.org/10.1016/j.epsl.2010.08.033

Silva, A., Baxter, C., Bryant, W., Bradshaw, A., & LaRosa, P. (2000). Stress-strain behavior and stress state of Gulf of Mexico clays in relation to slope processes. *Paper presented at 2000 Offshore Technology Conference, Offshore Technology Conference, Houston, TX*. https://doi.org/10.4043/12091-MS

Skarke, A., Ruppel, C., Kodis, M., Brothers, D., & Lobecker, E. (2014). Widespread methane leakage from the sea floor on the northern US Atlantic margin. *Nature Geoscience*, *7*, 657–661. https://doi.org/10.1038/ngeo2232

Sloan, E. D. (1998). *Clathrate hydrates of natural gases* (2nd ed.). New York, NY: Marcel Dekker.

Stranne, C., O'Regan, M., & Jakobsson, M. (2017). Modeling fracture propagation and seafloor gas release during seafloor warming-induced hydrate dissociation. *Geophysical Research Letters*, *44*(16), 8510–8519. https://doi.org/10.1002/2017GL074349

Sultan, N., Bohrmann, G., Ruffine, L., Pape, T., Riboulot, V., Colliat, J.-L., et al. (2014). Pockmark formation and evolution in deep water Nigeria: Rapid hydrate growth versus slow hydrate dissolution. *Journal of Geophysical Research*, *119*(4), 2679–2694. https://doi.org/10.1002/2013JB010546

Sun, Y., Wu, S., Dong, D., Lüdmann, T., & Gong, Y. (2012). Gas hydrates associated with gas chimneys in fine-grained sediments of the northern South China Sea. *Marine Geology*, *311–314*, 32–40. https://doi.org/10.1016/j.margeo.2012.04.003

Thatcher, K. E., Westbrook, G. K., Sarkar, S., & Minshull, T. A. (2013). Methane release from warming-induced hydrate dissociation in the West Svalbard continental margin: Timing, rates, and geological controls. *Journal of Geophysical Research Solid Earth*, *118*(1), 22–38. https://doi.org/10.1029/2012JB009605

Torres, M. E., McManus, J., Hammond, D. E., de Angelis, M. A., Heeschen, K. U., Colbert, S. L., et al. (2002). Fluid and chemical fluxes in and out of sediments hosting methane hydrate deposits on Hydrate Ridge, OR, I: Hydrological provinces. *Earth and Planetary Science Letters*, *201*(3-4), 525–540. https://doi.org/10.1016/S0012-821X(02)00733-1

Tréhu, A. M., Flemings, P. B., Bangs, N. L., Chevallier, J., Gràcia, E., Johnson, J. E., et al. (2004). Feeding methane vents and gas hydrate deposits at south Hydrate Ridge. *Geophysical Research Letters*, *31*, L23310. https://doi.org/10.1029/2004GL021286

Tryon, M. D., Brown, K. M., & Torres, M. E. (2002). Fluid and chemical fluxes in and out of sediments hosting methane hydrate deposits on Hydrate Ridge, OR, II: Hydrological processes. *Earth and Planetary Science Letters*, *201*(3–4), 541–557. https://doi.org/10.1016/S0012-821X(02)00732-X

Velde, B. (1996). Compaction trends of clay-rich deep sea sediments. *Marine Geology*, *133*(3–4), 193–201. https://doi.org/10.1016/0025-3227(96)00020-5

Waite, W. F., Santamarina, J. C., Cortes, D. D., Dugan, B., Espinoza, D. N., Germaine, J. T., et al. (2009). Physical properties of hydrate-bearing sediments. *Reviews of Geophysics*, *47*, RG4003. https://doi.org/10.1029/2008RG000279

Warpinski, N. R., & Branagan, P. T. (1989). Altered-stress fracturing. *Journal of Petroleum Technology*, *41*(9), 990–997. https://doi.org/10.2118/17533-PA

Warpinski, N. R., & Teufel, L. W. (1987). Influence of geologic discontinuities on hydraulic fracture propagation. *Journal of Petroleum Technology*, *39*(2), 209–220. https://doi.org/10.2118/13224-PA

Washburn, E. W. (1921). The dynamics of capillary flow. *Physical Review*, *17*(3), 273–283. https://doi.org/10.1103/PhysRev.17.273

Weinberger, J. L., & Brown, K. M. (2006). Fracture networks and hydrate distribution at Hydrate Ridge, Oregon. *Earth and Planetary Science Letters*, *245*, 123–136. https://doi.org/10.1016/j.epsl.2006.03.012

Wojtanowicz, A. K., Bourgoyne, A. T., Zhou, D., & Bender, K. (2000). *Strength and fracture gradients for shallow marine sediments* (Final Technical Report). Herndon, VA: U. S. Department of Interior.

Wood, W. T., Gettrust, J. F., Chapman, N. R., Spence, G. D., & Hyndman, R. D. (2002). Decreased stability of methane hydrates in marine sediments owing to phase-boundary roughness. *Nature*, *420*(6916), 656–660. https://doi.org/10.1038/nature01263

Xu, W., & Germanovich, L. N. (2006). Excess pore pressure resulting from methane hydrate dissociation in marine sediments: A theoretical approach. *Journal of Geophysical Research*, *111*(B1), B01104. https://doi.org/10.1029/2004JB003600

Yan, C., Deng, J., Lai, X., Li, X., & Feng, Y. (2015). Borehole stability analysis in deepwater shallow sediments. *Journal of Energy Resources Technology*, *137*(1), 012901. https://doi.org/10.1115/1.4027564

You, K., Flemings, P. B., Malinverno, A., Collett, T. S., & Darnell, K. (2019). Mechanisms of methane hydrate formation in geological systems. *Reviews of Geophysics*, *57*(4), 1146–1196. https://doi.org/10.1029/2018RG000638

Zoback, M. D. (2007). *Reservoir geomechanics*. Cambridge, UK: Cambridge University Press.

Zühlsdorff, L., & Spiess, V. (2004). Three-dimensional seismic characterization of a venting site reveals compelling indications of natural hydraulic fracturing. *Geology*, *32*(2), 101–104. https://doi.org/10.1130/G19993.1